# Magnetism and transport in $Pr_{1-x}Sr_xMnO_3$ single crystals ($0.48 \leqslant x \leqslant 0.57$)

J. Hejtmánek, E. Pollert, Z. Jirák, D. Sedmidubský, and A. Strejc
*Institute of Physics of ASCR, Cukrovarnická 10, 162 53 Prague 6, Czech Republic*

A. Maignan, Ch. Martin, and V. Hardy
*Laboratoire CRISMAT, ISMRA et Université de Caen, 6, Boulevard du Maréchal Juin, 14050 Caen, France*

R. Kužel
*Faculty of Mathematics and Physics, Charles University in Prague, Ke Karlovu 3, 121 16 Prague 2, Czech Republic*

Y. Tomioka
*Joint Research Center for Atom Technology (JRCAT), Tsukuba 305-0046, Japan*
(Received 6 November 2001; revised manuscript received 13 March 2002; published 15 July 2002)

The magnetic, electric, and thermal transport properties of the single-crystal $Pr_{1-x}Sr_xMnO_3$ perovskites have been investigated in the compositional region $0.48 \leqslant x \leqslant 0.57$. The end compositions are characterized as ideal examples of the ferromagnetic ($T_C = 290$ K) and the A-type antiferromagnetic ($T_N = 215$ K) metals with a strong quadratic temperature dependence of the electrical resistivity below $T_C$ ($T_N$), respectively. A transient behavior is observed on two intermediate samples with $x \cong 0.5$, which are ferromagnetic below $T_C = 265$ K and undergo a second transition to antiferromagnetism at $T_N = 125$–$155$ K. Appreciable magnetoresistance effects in these samples below $T_N$ are attributed to the field-induced antiferromagnetic⇒ferromagnetic phase transition. A detailed comparison of observed magnetothermal and magnetoelectrical conductivities justifies the application of Wiedemann–Franz law and points to an important role of electronic contribution in the thermal transport.

DOI: 10.1103/PhysRevB.66.014426 PACS number(s): 75.40.Cx, 71.28.+d, 72.15.Jf

## I. INTRODUCTION

The phase diagrams of perovskite manganites $Ln^{3+}_{1-x}A^{2+}_xMnO_3$ (Ln-rare earth, A-Alkaline earth) display a large variety of magnetic arrangements. In a narrow compositional window of $0.45 \leqslant x \leqslant 0.6$, two systematic trends in the evolution of magnetic structures are observed with respect to the steric and electronic effects. These are generally parametrized by the average Ln,A size and Mn valency: (i) for large size of Ln,A cations the increasing $x$ induces ground states in the sequence of ferromagnetic metallic, A-type antiferromagnetic and C-type antiferromagnetic arrangements[1,2] while, (ii), for the fixed $x$ the decrease of the average size of Ln,A cations leads to the replacement of the A-type by the CE-type magnetic order.[2,3] Both the CE- and C-type antiferromagnets are electrically nonconducting and orbital polarization of localized $e_g$ electrons is of the $d_{3r^2-z^2}$ kind. In contrast, the A-type antiferromagnets exhibit a high electrical conductivity below $T_N$ and orbital polarization of itinerant $e_g$ electrons is of the $d_{x^2-y^2}$ kind. The detailed magnetic and magnetotransport study of the A-type antiferromagnetic $Nd_{0.45}Sr_{0.55}MnO_3$ single crystal of orthorhombic symmetry revealed, moreover, that the electrical conductivity below $T_N$ is strongly anisotropic—highly conducting in ferromagnetic planes and insulating perpendicularly.[4] As the presented perovskites $Pr_{1-x}Sr_xMnO_3$ concerned, the single crystal data covering the relevant composition region are still lacking. We thus report on the magnetism, electronic, and thermal properties of four crystals with $x = 0.48$, 0.49, 0.50, and 0.57. Based on electrical and thermal transport data we experimentally demonstrate the validity of Wiedemann–Franz law and, in particular, the quasi-two-dimensional metallic character of electrical conductivity of the $Pr_{0.43}Sr_{0.57}MnO_3$ crystal.

## II. EXPERIMENT

Using both floating zone and high temperature-flux methods we have prepared four groups of $Pr_{1-x}Sr_xMnO_3$ single crystals. The crystals with $x = 0.49$ and 0.50 were prepared using floating-zone furnace equipped with hemiellipsoidal mirrors and halogen lamps as heat sources—a more detailed description was published previously.[5] For the study the cylindrical specimens with the diameter of $\simeq 4$ mm and length of $\simeq 5$–$8$ mm were cut and both the electrical and thermal gradients for transport studies were applied along the cylinder axis. With respect to the high temperature used in the case of the floating zone technique these crystals were post-annealed in flowing oxygen at 850 °C for 72 h..

The compounds with $x = 0.48$ and $x = 0.57$ were synthesized using high temperature flux method.[6] Crystals extracted from the flux were cube-shaped with approximate dimensions of $2 \times 2 \times 2$ mm and no additional heat treatment was applied before the measurements. The attempt to orient the electrical and thermal gradients with respect to crystallographic symmetry was unsuccessful and thus observed experimetal data are averaged through all crystallographic directions. Electron microprobe analysis of all studied crystals revealed very good homogeneity and the cation ratio (Pr+Sr)/Mn was determined as $1.00 \pm 0.015$.

The x-ray experiments were performed using Cu $K\alpha$ radiation on a diffractometer Siemens D500 with a helium

 

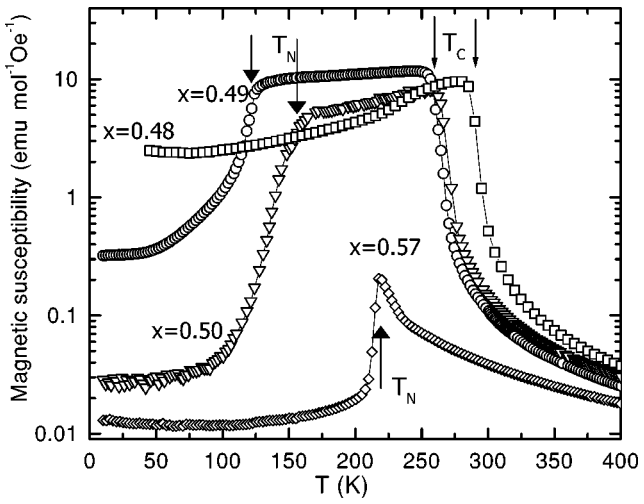


FIG. 1. The temperature dependence of magnetic susceptibility for $Pr_{1-x}Sr_xMnO_3$ single crystals (warming). The chemical composition is labeled.

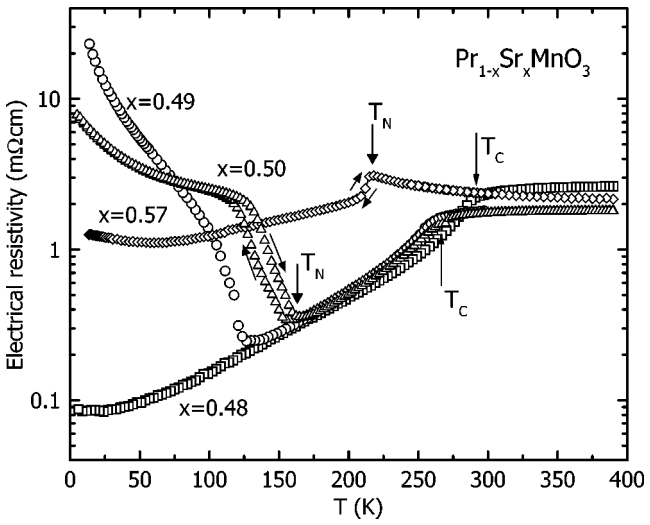


FIG. 2. The temperature dependence of electrical resistivity for single crystals of the $Pr_{1-x}Sr_xMnO_3$ series. The chemical composition and Curie (Néel) temperatures are labeled.

cooled chamber Oxford Instruments. The diffraction patterns ($2\Theta = 10° - 140°$) were collected with the Brown position sensitive detector between 20 and 300 K. The magnetoresistance, dc magnetization, and specific heat measurements were performed with a Quantum Design PPMS system. The magnetic susceptibility data were collected with a Quantum Design superconducting quantum interference device when applied magnetic field $h_{ac}$ was within the range of 1 Oe $\leqslant h_{ac} \leqslant 10$ Oe and excitation frequency between 100 and 1000 Hz.

The thermoelectric power and thermal conductivity measurements were carried out between 11 and 320 K using a close-cycle refrigerator. The four-point steady-state method was applied in order to eliminate thermal resistances between the sink and the heater. The experimental setup was checked using reference samples and for more detail we refer to Ref. 7. Particular difficulties were encountered in the case of $x = 0.57$ crystal because its small size does not allow one to simply attach four transport leads simultaneously with the heater. The sample was thus mounted on a Plexiglas TM support and the thermal conductivity of the crystal was extracted using calibrated thermal conductivity of plexiglass support.

### III. RESULTS

The magnetic susceptibility data in $Pr_{1-x}Sr_xMnO_3$ crystals are displayed in Fig. 1. The crystals with $x = 0.48$, 49, and 50 are ferromagnetic (FM) with $T_C$ of 290, 262, and 267 K, respectively. Upon cooling, in agreement with previously published data, the FM ground state is replaced for $x \geqslant 0.49$ by the A-type antiferromagnetic (AFM) one.[1,5,8] The Néel temperature $T_N$, characterized by a steep decrease of magnetic susceptibility, increases with Sr concentration from 124 K for $x = 0.49$ to 215 K for $x = 0.57$. Concurrently with increasing $T_N$ the low temperature susceptibility decreases with increasing $x$ and remains very low down to the lowest temperatures.

The temperature dependence of electrical resistivity is shown in Fig. 2. The weakly temperature dependent resistivity in the paramagnetic state for all samples is consistent with adiabatic hopping of polaronic carriers.[9] A more pronounced temperature activation of electrical resistivity above the $T_N$ for $x = 0.57$ crystal is likely linked with increased tetragonal deformation of the $MnO_6$ array as seen on Fig. 3. Here the temperature variation of lattice parameters of the

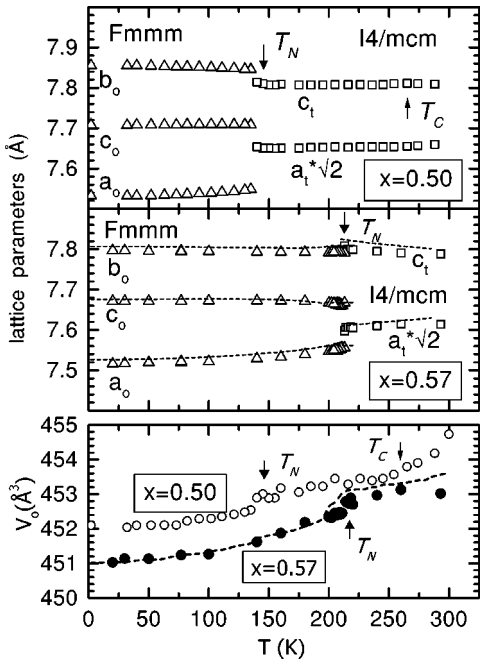


FIG. 3. The temperature dependence of lattice parameters for single-crystal $Pr_{0.43}Sr_{0.57}MnO_3$, (△,□) and $Pr_{0.4}Sr_{0.60}MnO_3$ ceramics (dashed line) are compared with $Pr_{0.5}Sr_{0.50}MnO_3$ ceramics (Ref. 3). In the lower panel the temperature evolution of the unit cell volume of $x = 0.57$ single crystal (●) and $x = 0.6$ ceramics (dashed line) is depicted in comparison with $x = 0.50$ ceramics (○).

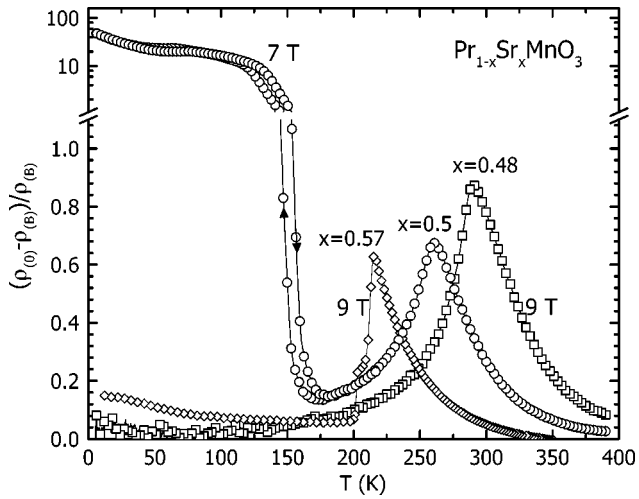


FIG. 4. The temperature dependence of the magnetoresistance expressed as $(\varrho_{(0)}-\varrho_{(B)})/\varrho_{(B)}$ at $B=9$ or 7 T for single crystals of the $Pr_{1-x}Sr_xMnO_3$ series. The chemical composition and Curie (Néel) temperatures are labeled in the graph.

$Pr_{0.43}Sr_{0.57}MnO_3$ crystal is displayed in comparison with data for the $x=0.50$ ceramics.[3] Upon cooling below 300 K the $x=0.57$ crystal shows an increase of the $c$ lattice parameter of the tetragonal $I4/mcm$ high temperature phase which is directly linked with gradually increasing C-type orbital $d_{3z^2-r^2}$ orbital polarization. This evolution is sharply broken at $T_N$ where the competitive $d_{x^2-y^2}$ orbital polarization develops and leads to the $Fmmm$ symmetry.[10] As demonstrated in the figures this concomitant structural, magnetic, and insulator–metal transition takes place abruptly at 215 K without any observable hysteresis within $\Delta T \simeq 1$ K.

By contrast, the onset of A-type antiferromagnetism for $x=0.49$ and 0.50 crystals is accompanied by a steep increase of electrical resistivity via a hysteretic two-phase region ($\Delta T \sim 20$ K). The low temperature values of electrical resistivity remain, however, of the order of $\rho_0 \sim 10$ m$\Omega$ cm and reflect the metallic-like conduction in two-dimensional (2D) FM planes. The A-type AFM order is, similarly as for $x=0.57$, accompanied by the structural transition and a decrease of the unit cell volume at $T_N$ as demonstrated in the Fig. 3. These attributes corroborate well with the first- order character of the FM⇔AFM transition. On the other hand, the smooth evolution of lattice parameters and unit cell volume across $T_C$ for the $x=0.50$ sample indicate that the magnetic transition is not strongly coupled with lattice and can be of second order.

The temperature dependence of magnetoresistance is further shown in Fig. 4. In the FM crystals the huge magnetoresistance peaks at $T_C$ and decreases symmetrically below and above $T_C$. The similar course of the magnetoresistance above $T_N$ in the $x=0.57$ crystal implies that the magnetic interactions are essentially the same as in FM crystals. The low temperature magnetoresistance is, however, substantially different for different crystals. In the case of FM metallic $x=0.48$ crystal, the magnetoresistance decreases smoothly to zero at 0 K. For the antiferromagnetic $x=0.50$ crystal, after a decrease below $T_C$, a huge low temperature magnetoresistance due to the magnetic-field-induced AFM ⇔FM transition is observed.[5] A small negative magnetoresistance smoothly increasing with decreasing temperature, detected for the $x=0.57$ sample below $T_N$, is likely associated with increased spin canting between antiferromagnetic layers which favors the interlayer tunneling.

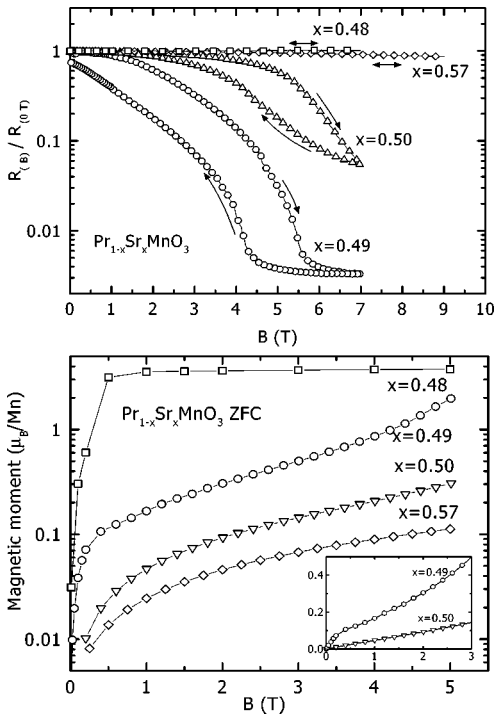


FIG. 5. Zero field cooled magnetoresistance (upper panel) and magnetic moment (lower panel) at 10 K for single crystals of the $Pr_{1-x}Sr_xMnO_3$ series. In the inset the difference between $x=0.49$ and $x=0.50$ crystals is demonstrated. A strong hysteresis of magnetoresistance encountered for $x=0.49$ and 0.50 crystals is absent for $x=0.48$ and 0.57 crystals.

The isothermal low temperature magnetoresitance is compared with magnetization in the Fig. 5. The negligible magnetoresistance of the $x=0.48$ crystal results from the complete magnetic polarization and, simultaneously, minimized impact of grain boundaries, which generally lead to negative magnetoresistance in ferromagnetic ceramic manganites. The huge magnetoresistance for the $x=0.49$ and 0.50 antiferromagnetic crystals is accompanied by simultaneous increase of the magnetic moment and corresponds to the magnetic-field-induced AFM⇔FM transition. The transition is completed for $x=0.49$ sample above 5.5 T while for $x=0.50$ only an onset of this phase transition is achieved at the same field. This observation indicates that the stability of 2D AFM with respect to the three-dimensional (3D) FM structure sharply increases with increasing $x$.

The evolution of the thermoelectric power with temperature is shown in Fig. 6. In the paramagnetic region the negative and almost temperature independent thermopower reflects the configurational entropy of hopping carriers.[7] The metallic nature of ferromagnetic phases in $x=0.48$–50 crystals is evidenced by a steep decrease of the thermopower magnitude below $T_C$ (Fig. 6) when the small and negative

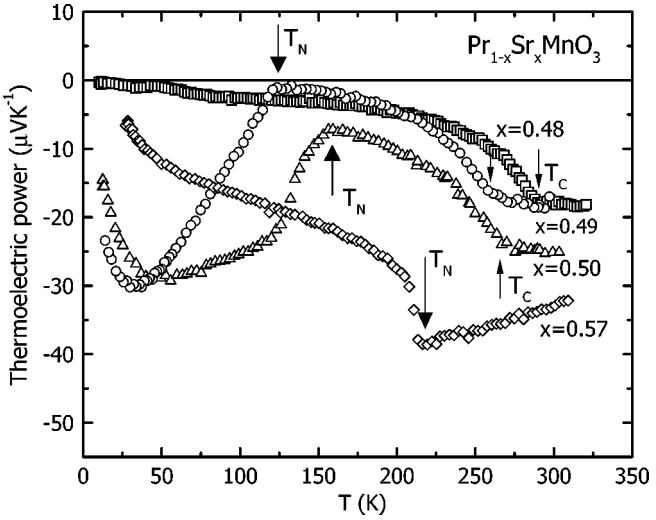


FIG. 6. The temperature dependence of thermoelectric power for single crystals of the $Pr_{1-x}Sr_xMnO_3$ series. The chemical composition and Curie (Néel) temperatures are labeled.

value for $x=0.48$ indicates ''electron'' like character of DOS at $E_F$ in distinction to hole-like behavior encountered in FM manganites with $x\sim 0.3$. The onset of antiferromagnetic order at $T_N=125$ and 155 K for $x=0.49$ and $x=0.50$ crystals, respectively, is characterized by an increasing magnitude of the thermopower down to $\simeq -30\ \mu V K^{-1}$. Contrary to that the magnitude of the thermopower decreases below $T_N=215$ K for the $x=0.57$ crystal. The final descent of the thermopower to zero at 0 K is encountered for all samples and is in conformity with the band-like character of carriers in the A-type AFM ground state. A smaller low temperature absolute value measured for $x=0.57$ crystal thus corroborates with its higher electrical conductivity.

The magnetic and magnetoresistive properties of the $x=0.57$ crystal were examined in detail in the vicinity of $T_N$ and the results are displayed in Figs. 7 and 8. The huge negative magnetoresistance together with the evolution of magnetic moment encountered above $T_N$ ($T=225$ K) reflect the overwhelming role of ferromagnetic interactions. The Brillouin fit, represented by the full line, provides very resonable parameters of hypothetical FM phase: Curie temperature $T_C\simeq 197$ K and the total spin value $S\simeq 2$. Just below $T_N$ ($T=200$ K) the 3D FM interactions vanish, the magnetoresistance sharply drops and only a small magnetoresistance linked with the interlayer canting persists. However, at a critical field $B\simeq 10$ T the metamagnetic AFM⇔FM phase transition occurs and is followed by ferromagnetic-like behavior. The impact of external magnetic field on the long-range AFM ordering temperature is exemplified in Fig. 8. Under the field of 14 T the onset of AFM order is shifted from 215 to $\simeq 190$ K, which contrasts with the data acquired on $x=0.49$ crystal where, even at lowest temperatures, the A-type structure is entirely converted to 3D FM phase by application of 7 T only. The robustness of AFM ground state of $Pr_{0.43}Sr_{0.57}MnO_3$ crystal is compared in the inset with data reported for

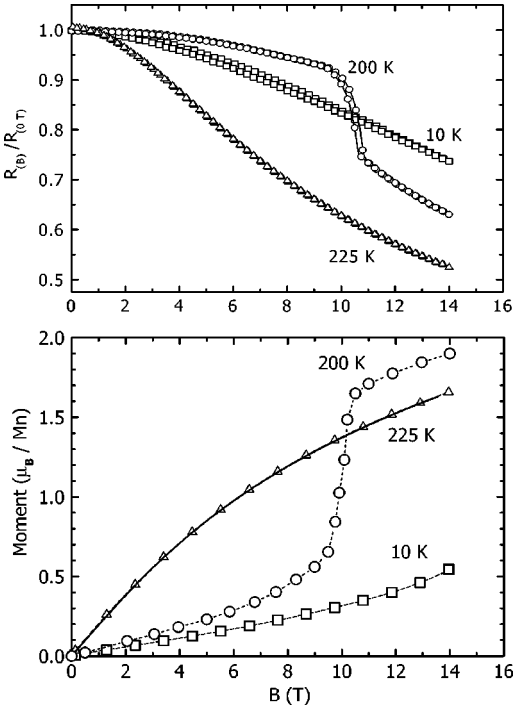


FIG. 7. Zero field cooled magnetoresistance (upper panel) and magnetic moment (lower panel) at various temperatures for $x=0.57$ single crystal. Note the metamagnetic transformation at 200 K for $B=\simeq 10$ T.

$Nd_{0.45}Sr_{0.55}MnO_3$ crystal with the same magnetic structure and hole concentration.[4]

The anomalies encountered in the temperature dependence of the thermal conductivity, shown in Fig. 9, demonstrate the essential interrelation between the thermal transport and magnetic transitions. Similarly as reported previously for $Pr_{0.5}Sr_{0.5}MnO_3$ ceramics, the simultaneous oc-

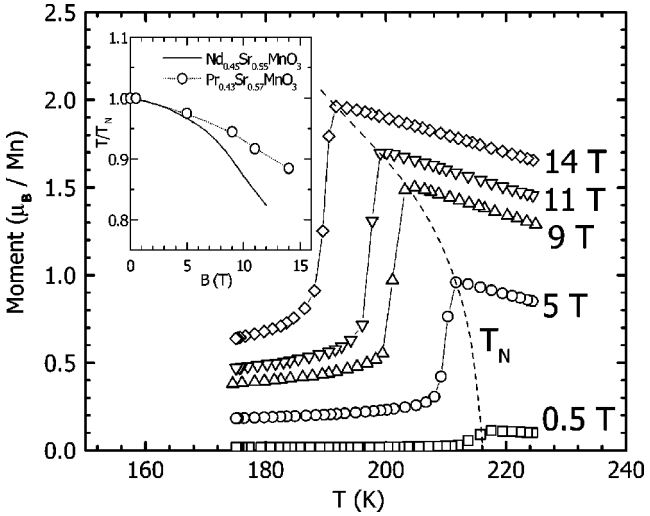


FIG. 8. The temperature dependence of magnetic moment in the vicinity of Néel temperature at various external fields for the $x=0.57$ single crystal. In the inset the shift of $T_N$ with magnetic field is compared with the data reported for $Nd_{0.45}Sr_{0.55}MnO_3$ single crystal (Ref. 4).

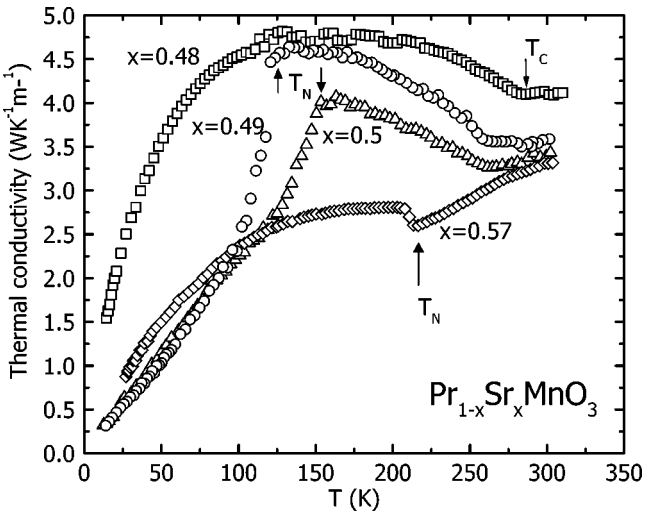


FIG. 9. The temperature dependence of the thermal conductivity for single crystals of the $Pr_{1-x}Sr_xMnO_3$ series. The chemical composition and Curie (Néel) temperatures are labeled.

currence of the ferromagnetic and metal-insulator transitions at $T_C$ in the $x=0.48$–50 crystals is accompanied by an enhancement of thermal conductivity.[11,12] For antiferromagnetic $x=0.49$ and $x=0.50$ crystals, however, the increase of thermal conductivity below $T_C$ is broken at $T_N$ by a precipitous descent. Upon further cooling below $\sim 100$ K the thermal conductivity sharply decreases and falls to very low values at low temperatures. In case of $x=0.57$ crystal the direct transition from the paramagnetic to antiferromagnetic state is accompanied by a small increase of thermal conductivity at $T_N=215$ K with the low temperature values being similar to that of $x=0.49$ and $x=0.50$ crystals.

## IV. DISCUSSION

### A. FM ⇔AFM phase boundary

The narrow phase boundary between FM and AFM ground states, observed at $x=0.49$, results in the presence of FM inclusions in the sample. Indeed, the extrapolated zero field magnetization of $\simeq 0.1\mu_B$ at 10 K in the $x=0.49$ crystal, shown in the inset of Fig. 5, corresponds to residual $\sim 3\%$ volume of FM phase. It is thus straightforward to relate the easiness of the magnetic-field-induced transition from AFM⇔FM phase with precursor role of such residual FM inclusions. This hypothesis is supported by substantially lower magnetoresistance and undetectable residual magnetization of the $x=0.50$ crystal which is already out of the boundary. Finely the $Pr_{0.43}Sr_{0.57}MnO_3$ crystal represents a rigid AFM structure. The low temperature magnetization and magnetoresistance (Fig. 7), however, is substantially smaller than of the analogous $Nd_{0.45}Sr_{0.55}MnO_3$; $R_{12\ T}/R_0 \simeq 0.8$ observed at 10 K for $Pr_{0.43}Sr_{0.57}MnO_3$ crystal contrasts with $R_{12\ T}/R_0 \simeq 0.43$ for $Nd_{0.45}Sr_{0.55}MnO_3$.[4] Simultaneously, a substantially lower impact of external magnetic field on $T_N$ of $Pr_{0.43}Sr_{0.57}MnO_3$ crystal is demonstrated in the inset of Fig. 8. The possible origin of this difference can be associated with slightly different crystal symmetries of $Pr_{0.43}Sr_{0.57}MnO_3$ and $Nd_{0.45}Sr_{0.55}MnO_3$ crystals. While the $Nd_{0.45}Sr_{0.55}MnO_3$ crystal exhibits the *Pbnm* symmetry with two symmetrically distorted Mn–O–Mn bond angles of 168° lying in conducting FM planes, the $Pr_{0.43}Sr_{0.57}MnO_3$ possesses the *Fmmm* symmetry with two Mn–O–Mn bond angles of 169° and 180° in conducting FM planes, respectively. Supposing a direct connection between the bonding symmetry and orbital polarization of $e_g$ electron, the straighten Mn–O–Mn bond angles in $Pr_{0.43}Sr_{0.57}MnO_3$ crystal can be at the root of both the higher electrical conductivity, linked with $d_{x^2-y^2}$ orbital polarization, and higher stability against the spin canting at low temperatures.

### B. Electrical transport

The weakly temperature dependent resistivity in paramagnetic state is coherent with adiabatic hopping of charge carriers. The hopping energy for $x=0.48$–0.50 samples is evaluated to $E_A \simeq 24$ meV. A more pronounced temperature activation of electrical resistivity above the $T_N$ for $x=0.57$ crystal corresponds $E_A \simeq 39$ meV. This fact is likely linked with the increased deformation of the $MnO_6$ array due to C-type orbital polarization, as seen in the middle panel of Fig. 3. The viability of adiabatic hopping as the transport mechanism is documented by temperature independent thermoelectric power data. As pointed out by Doumerc the fact that the conducting electron can adopt different spin state with respect to the spin background provides additional degree of freedom.[13] Thus the conventional Heikes formula-$S=-k_B/|e|\ln\{(1-x)/x\}$-($x=n/N$, $N$ the number of available sites and $n$ the number of charge carriers) which reflects solely the contribution of configurational entropy of singly occupied states, i.e., for a strong on-site Coulomb repulsion, the modified expression $S=-k_B/|e|\ln\{\beta_S(1-x)/x\}$ is more appropriate to use. The spin degree of freedom $\beta_S$ amounts to $[2S_{Mn^{3+}}+1]/[2S_{Mn^{4+}}+1]=5/4$ and provides additional spin thermopower of $-19.2\ \mu V\,K^{-1}$. Indeed, as for $x \simeq 0.50$ the simple configurational entropy should result in zero thermopower, we observe good agreement between theoretical spin thermopower and experimental values which vary between $-18\ \mu V\,K^{-1}$ ($x=0.48$) and $-25\ \mu V\,K^{-1}$ for $x=0.50$. In the case of $x=0.57$ crystal the increase of the absolute value of thermopower at room temperature to $\simeq -30\ \mu V\,K^{-1}$ likely reflects the increase of the configurational entropy of hopping electrons due to decreased concentration of the $e_g$ electrons. A small temperature activation of thermopower down to $T_N$ points to a pronounced tendency to the charge carrier localization which is consistent with the temperature activated resistivity.

In order to discriminate between itinerant and localized picture of charge carrier transport the $k_F l$ product ($l$ is the mean free path of charge carriers and $k_F$ is the Fermi wave vector) can be considered. This value can be estimated on the basis of an assumption $k_F l=[\hbar(3\pi^2)^{2/3}]/(e^2\varrho n^{1/3})$, where $e$ is the electronic charge and $n$ is the number of charge carriers. Taking the $n$ as a total number of $e_g$ electrons, i.e., $n \simeq 0.9\times 10^{28}$ m$^{-3}$ for $x\sim 0.5$, the room temperature resistivities of $\sim 2.5$ m$\Omega$ cm yield $k_F l=0.7$, which corroborates well with the above-mentioned model of hopping conduc-

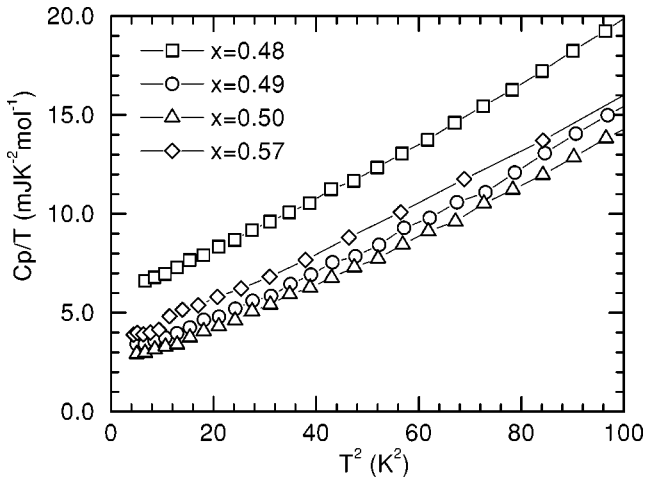


FIG. 10. The temperature dependence of the specific heat for $Pr_{1-x}Sr_xMnO_3$ single crystals shown as $C/T$ vs $T^2$ plot.

tion. On the other hand, in the ferromagnetic metallic state ($x=0.48$) the residual resistivity of $\sim 80\ \mu\Omega$ cm provides $k_F l = 23$ which is clearly in favor to a metallic picture of low-temperature conductivity. Supposing the two-dimensional metallic conductivity in FM planes for $x=0.57$ crystal, the experimental value of residual conductivity makes the sheet conductivity $\sigma_0 = d/\varrho_0 = 3.8\times 10^{-5}[\Omega^{-1}]$ ($d$ is the spacing of FM layers $\simeq 3.8$ Å and $\varrho_0 = 1\ \text{m}\Omega\,\text{cm}$ is the residual resistivity), while the theoretical criterion of metallic conductivity in 2D $\sigma_{\min} = e^2/2\pi\hbar = 3.87\times 10^{-5}[\Omega^{-1}]$ locates the crystal just at the border of metallic conductivity. The mean free path given by the ratio $\sigma_0/\sigma_{min} = k_F l \sim 1$ further indicates that the sample occurs at the limit of a weak localization. This fact is likely responsible for a small resistivity upturn observed below 50 K. Much higher electrical resistivity observed for $x=0.49$ and 0.50 crystals at low temperatures implies that $k_F \ll 1$ already involving hopping conduction.

In the $x=0.48$ ferromagnetic crystal the electrical resistivity below $T_C$ is dominated by quadratic $A\ T^2$ term, which is an indication of $e-e$ correlations. The observed constant $A \sim 7\ \text{n}\Omega\,\text{cm}\,\text{K}^{-2}$ is similar to that determined in optimally doped $La_{0.67}(Pb,Ca)_{0.33}MnO_3$ single crystals by Jaime *et al.*[9] In a simple case the quadratic term $A$ is related to the electronic specific heat coefficient $\gamma$ by empirical Kadowaki–Woods ratio $A/\gamma^2 = 1\times 10^{-5}\ \mu\Omega\,\text{cm}(\text{mol K/mJ})^2$. Supposing the validity of such ratio, a large electronic specific heat term $\gamma \simeq 26\ \text{mJ}\,\text{K}^{-2}\text{mol}^{-1}$ should be anticipated. Thus, in order to assess the character of charge carriers at $E_F$, we have measured the low temperature specific heat. The data are shown as $C_p/T$ vs $T^2$ in Fig. 10. The experimentally observed values of the linear electronic term $\gamma$ for $x=0.48$ are very similar to that reported in the literature and amount to $\simeq 5\ \text{mJ}\,\text{K}^{-2}\ \text{mol}^{-1}$.

Surprisingly, the analysis of electrical resistivity of antiferromagnetic $x=0.57$ crystal below $T_N$ unveils also the dominating quadratic $A\ T^2$ term. An estimation of hypothetical electronic specific heat using Kadowaki–Woods ratio provides $\gamma \simeq 55\ \text{mJ}\ \text{K}^{-2}\ \text{mol}^{-1}$, which contrasts even more with experimental value of $\gamma \simeq 3.0\ \text{mJ}\,\text{K}^{-2}\ \text{mol}^{-1}$. Consequently, with respect to the observed specific heat data, more effective electron–electron correlations limiting critically the carrier mean free path $l$ in ferromagnetically polarized state should be anticipated. Most likely these correlations are mediated by Jahn–Teller phonons and/or spin excitations.[9]

The uniformity of the electronic term $\gamma$ determined for $x=0.49$, 0.50, and $x=0.57$ antiferromagnetic crystals contrasts with the diversity of their low temperature electrical resistivities and thermoelectric power. Taking into account the low absolute value of the thermopower the origin of pronounced localization for $x=0.49$ and $x=0.50$ is not due to an increased effective mass $m^*$, as one expects for strong electronic correlations, but more likely due to the concurrence of the ''charge commensurability'' at half-filling and orbital polarization accompanied by the structural deformation, which confines the double-exchange electron transfer in the conducting FM planes and forms a ''pseudogap'' at $E_F$ in the $Pr_{1-x}Sr_xMnO_3$ system for $x \sim 0.50$. In relation to the existence of the ''pseudogap'' in highly doped manganites this was experimentally observed in layered homologues $La_{3-x}Sr_xMn_2O_7$ with the ratio $Mn^{3+}/Mn^{4+} \simeq 1$.[14] The pseudogap, at least partial, closing for $x=0.57$ crystal is likely linked to the loss of the ''charge commensurability'' and lowered deformation of FM planes which possibly results in higher electrical conductivity and typical metallic-like thermopower.

### C. Thermal transport

An experimental estimate of the Lorenz ratio $L_e$ can be made by simultaneous analysis of the thermal conductivity and electrical resistivity data in the vicinity of ferromagnetic transition temperature $T_C$. We can write:

$$\lambda_{total} = \lambda_{electron} + \lambda_{phonon} \ \text{ with } \ \lambda_{electron} = L_e T/\varrho, \quad (1)$$

where $\varrho$ is electrical resistivity. The differentiation in temperature provides

$$\frac{d\lambda_{total}}{dT} = \frac{d\lambda_{ph}}{dT} + \frac{L_e}{\varrho} - \frac{L_e T}{\varrho^2}\frac{d\varrho}{dT}. \quad (2)$$

Based on the unchanged crystal structure and apparent second-order character of magnetic transition one may suppose that the phonons only contribute to a smooth temperature dependence of $\lambda$ over $T_C$ and the temperature anomalies at $T_C$ in both $\varrho(T)$ (Fig. 2) and $\lambda(T)$ (Fig. 9) are solely driven by critical scattering of electrons. The analysis in the vicinity of $T_C$ for $Pr_{0.52}Sr_{0.48}MnO_3$ crystal provides an average value $L_e^{290\ \text{K}} \simeq 3.6\times 10^{-8}\ \text{W}/\Omega\ K^2$ which exceeds the theoretical Lorenz number $L_o = 2.44\times 10^{-8}\ \text{W}/\Omega\ \text{K}^2$. Nonetheless, this estimation appears false in view of further discussion in the following.

More reliable experimental estimation of the Lorenz number $L_e$ provides the analysis of magnetothermal conductivity and magnetoresistance. The compilation of magnetothermal and magnetoresistance data acquired on the $Pr_{0.50}Sr_{0.50}MnO_3$ single crystal and ceramics are shown in Fig. 11 where, in addition, the data for ferromagnetic $Pr_{0.65}Sr_{0.14}Ca_{0.21}MnO_3$

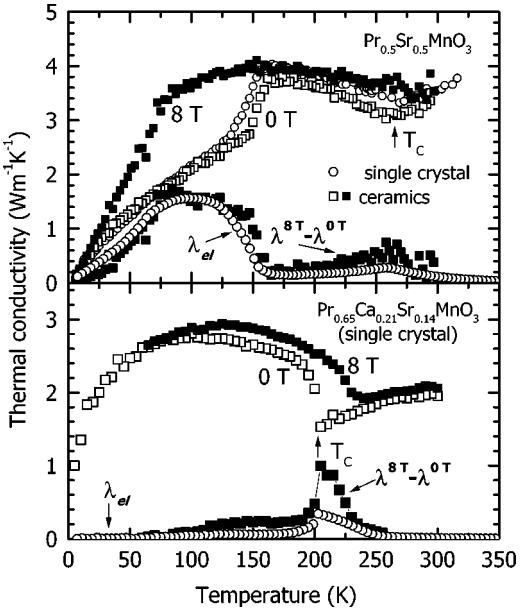


FIG. 11. The temperature dependence of the thermal conductivity for 0 and 8 T for $Pr_{0.50}Sr_{0.50}MnO_3$ (upper panel) and $Pr_{0.65}Sr_{0.14}Ca_{0.21}MnO_3$ (lower panel). To enable the comparison the ceramic data were corrected on the porosity. Using Wiedemann–Franz law with $L_o$ and the magnetotransport data yielded on single crystals the calculated magnetoelectronic contribution $\lambda_{el}$ (○) is compared with experimental magnetothermal conductivity $\lambda_{mag}=\lambda^{8\ T}-\lambda^{0\ T}$ (■).

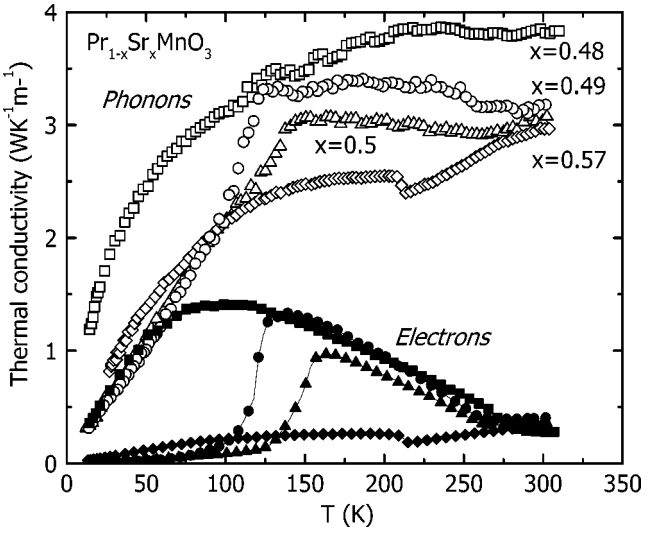


FIG. 12. The decomposition of the total thermal conductivity on the phonon and electron parts, respectively. The chemical composition of $Pr_{1-x}Sr_xMnO_3$ single crystals is labeled.

single crystal ($T_C=204$ K) are also presented in the lower panel. The relevance of the analysis with the use of magnetothermal data acquired on ceramic specimen is substantiated by the comparison of the ceramic and single-crystal zero-field data which are, apart from a small experimental fluctuation, practically identical. The experimentally observed magnetothermal conductivity $\lambda^{mag}=\lambda^{8\ T}-\lambda^{0\ T}$ for $Pr_{0.65}Sr_{0.14}Ca_{0.21}MnO_3$ single crystal exceeds in the vicinity of $T_C$ significantly the magnetoelectronic contribution calculated using Wiedemann–Franz law with $L_o$. This observation is coherent with the first-order character of ferromagnetic transition, which points to a strong magnetoelastic coupling.[15] Further on, supposing the validity of Wiedemann–Franz law with ideal $L_o$, the total magnetothermal conductivity of $Pr_{0.50}Sr_{0.50}MnO_3$ below $T_N$, connected with magnetically induced AFM-FM transition, can be associated entirely with magnetoelectronic component. Moreover, supposing the Lorenz number exceeding the $L_o$, the calculated magnetoelectronic component would exceed the experimentally observed total magnetothermal contribution. We thus conclude that apparent second-order FM transition in the $x=0.48$ crystal is still associated with a small enhancement of $\lambda_{phonon}$ in the vicinity of $T_C$ and, consequently, the use of Lorenz free number $L_o$ for the evaluation of $\lambda_{electron}$ is the most appropriate.

Thus using the Wiedemann–Franz law with $L_o$ the evaluation of the phonon part of thermal conductivity is shown in Fig. 12 when, based on our previous study, the eventual magnon contribution to thermal conductivity was omitted.[7] The electronic contribution $\lambda_{electron}$ represents a substantial part of the heat transport in ferromagnetic crystal $x=0.48$ only at low temperatures while this contribution in the AFM crystals $x=0.49$–$0.57$ is negligible. Furthermore in accordance with changes of lattice parameters (Fig. 7) we differentiate between the negligible variation of $\lambda_{phonon}$ over the $T_C$ and the anomalies detected at $T_N$. Since the phonon part of thermal conductivity is a product of specific heat, sound velocity and mean free path of phonons $l_{phonon}$ and since the first two quantities do not manifest such changes which could explain observed anomalies, we presume that the observed decrease of $\lambda_{phonon}$ below $T_N$ for the $x=0.49$ and 0.50 and increase for $x=0.57$ crystals reflect predominantly changes in the mean free path of phonons. In the first case we suggest that a strong magnon scattering via magnetoelastic coupling is a reason for the decreased $l_{phonon}$ in AFM phase with respect to the FM one.[15] In the second case the small step-like increase for $x=0.57$ crystal is a natural consequence of the mean free path revival due to the accomplished structural transition below $T_N$. The similar absolute values of $\lambda_{phonon}$ in the AFM phases at low temperatures are in conformity with identical crystal and magnetic structures and the substantially smaller low temperature value of $\lambda_{phonon}$ compared to FM crystal $x=0.48$ is associated with an enhanced magnon scattering.

## V. CONCLUSIONS

The magnetic, electric, and thermal transport properties of the single-crystal perovskites $Pr_{1-x}Sr_xMnO_3$ have been investigated in the region of the FM–AFM transition, i.e., $0.48\leqslant x\leqslant 0.57$. The analysis of the experimental data leads to the following conclusions: (i) independent of the magnetic order all samples are electron-like conductors at low temperatures, (ii) the sharp phase boundary between the ferromagnetic 3D metal and A-type antiferromagnetic ground states is observed at $x=0.49$, (iii) the low temperature CMR effect in the antiferromagnetic A-type phase is linked to a

presence of residual ferromagnetic inclusions promoting the expansion of 3D FM order under external magnetic field, (iv) without apparent variation in the crystal, magnetic and orbital structures, the low temperature electrical conductivity is substantially enhanced when increasing $x$ from 0.49 to 0.57 reaching just the limit of the 2D metallic conductivity, (v) within the same A-type AFM structure the higher $T_N$ and increased metallicity below $T_N$ reflect an increased strength of double-exchange FM interactions within the conducting planes, which scales, in a first approximation, with an increase of tolerance factor from $t=0.939(x=0.49)$ to $t=0.948(x=0.57)$, (vi) the simultaneous transport and specific heat investigations suggest that hindered charge carrier transport in the 2D AFM phases is not simply associated with a lowered mean free path; a more plausible explanation relates this effect to an interplay of the lowered dimensionality, $N(E_F)$, and extremely short mean free path of charge carriers, which is indicated both in the thermal and electrical conductivity data, and (vii) the experimentally determined Lorenz number $L_e(T)$ amounts to $L_o$ which justifies the application of the Wiedemann–Franz law.

## ACKNOWLEDGMENTS

We are grateful to Dr. S. Krupička for stimulating discussions. The authors acknowledge the financial support of the Grant Agency of the Czech Republic (Grant No. 202-99/0413), Grant Agency of the Academy of Sciences the Czech Republic (Grants Nos. D101 0023 and A101 0004/00).

[1] C. Martin, A. Maignan, M. Hervieu, and B. Raveau, Phys. Rev. B **60**, 12191 (1999).
[2] Y. Moritomo, T. Akimoto, A. Nakamura, K. Ohoyama, and M. Ohashi, Phys. Rev. B **58**, 5544 (1998).
[3] F. Damay, thesis, Universite de Caen, CRISMAT, 1999.
[4] H. Kuwahara, T. Okuda, Y. Tomioka, A. Asamitsu, and Y. Tokura, Phys. Rev. Lett. **82**, 4316 (1999).
[5] Y. Tomioka, A. Asamitsu, Y. Moritomo, H. Kuwahara, and Y. Tokura, Phys. Rev. Lett. **74**, 5108 (1995).
[6] E. Pollert, Z. Jirák, M. Maryško, and J. Hejtmánek, J. Magn. Magn. Mater. (in press).
[7] J. Hejtmánek, Z. Jirák, M. Maryško, C. Martin, A. Maignan, M. Hervieu, and B. Raveau, Phys. Rev. B **60**, 14057 (1999).
[8] H. Kawano, R. Kajimoto, H. Yoshizawa, Y. Tomioka, H. Kuwahara, and Y. Tokura, Phys. Rev. Lett. **78**, 4253 (1995).
[9] M. Jaime, P. Lin, M. B. Salamon, and P. D. Han, Phys. Rev. B **58**, 5901 (1998).
[10] Contrary to $Nd_{0.45}Sr_{0.55}MnO_3$ which retains the $Pbnm$ symmetry below $T_N$, the change of the $I4/mcm$ to $Fmmm$ symmetry in $Pr_{1-x}Sr_xMnO_3$ crystals over the FM–AFM transition implies a formation of microscopic twins thus making it impossible to distinguish macroscopically the transport anisotropy. Nonetheless the large anisotropy in charge carrier transport in the A-type antiferromagnetic state, metallic in FM planes and insulating perpendicularly, leads to the direct association of the measured data with the transport within the FM planes.
[11] J. L. Cohn, J. J. Neumier, C. P. Popoviciu, K. J. McClellan, and Th. Leventouri, Phys. Rev. B **56**, R8495 (1997).
[12] J. Hejtmánek, Z. Jirák, Z. Arnold, M. Maryško, S. Krupička, C. Martin, and F. Damay, J. Appl. Phys. **83**, 7204 (1998).
[13] J. P. Doumerc, J. Solid State Chem. **110**, 419 (1994).
[14] D. B. Romero, Y. Moritomo, J. F. Mitchell, and H. D. Drew, Phys. Rev. B **63**, 132404 (2001).
[15] H. Fujishiro, M. Ikebe, T. Kikuchi, and H. Ozawa, Physica B **281&282**, 491 (2000).